Fault-tolerant Axial Flux Coreless PM Machines with Independent Phase Modules

Yaser Chulaee, Ali Mohammadi, Matin Vatani, and Dan M. Ionel
SPARK Laboratory, Stanley and Karen Pigman College of Engineering, University of Kentucky, Lexington, KY, USA
yaser.chulaee@uky.edu, alimohammadi@uky.edu, matin.vatani@uky.edu, and dan.ionel@ieee.org

***Abstract*—In this paper, a fault-tolerant two-phase high power coreless axial flux PM (AFPM) machine with a modular structure is introduced. The performance of this machine, in terms of torque, power density, and efficiency, is compared with its three-phase counterpart configuration based on finite element analysis (FEA) and experimental results. The fault tolerance of these two configurations, considering the control systems, is also compared. A detailed power loss breakdown for the prototype two-phase and three-phase printed circuit board (PCB) stator coreless AFPM machines derived from experiments is presented, showcasing that the introduced fault-tolerant two-phase machine has comparable performance and efficiency, while the phase windings are electrically insulated and magnetically decoupled. The common configurations for controlling a two-phase machine, namely four-leg and three-leg two-phase inverters, are also discussed along with the experimental results.**

***Index Terms*—Axial flux PM machines, coreless AFPM, PMSM, drive systems, fault-tolerance, PCB stator, multi-phase motors, finite element anlaysis, FEA, electric aircraft.**

I. Introduction

Permanent magnet synchronous machines (PMSMs), especially those of the axial flux type, are currently being researched and developed for diverse systems such as HVAC, aviation propulsion, and electric vehicle [1], [2]. Coreless (air-cored) stator axial flux permanent magnet (AFPM) machines belong to this category of electric machines, providing some benefits through the elimination of magnetic cores and the associated losses [3]. These advantages consist of zero cogging torque, minimized audible noise and vibration, along with reduced mass and volume [4], [5]. These attributes contribute to an improved efficiency and torque density. The potentially high torque density and absence of frequency-dependent core losses make coreless AFPM machines a promising candidate for electric aircraft propulsion applications that demand high speed operation and power density [6].

The lack of a magnetic core creates an opportunity to incorporate printed circuit board (PCB) stators into coreless AFPM machines. Printed circuit board stators have gained popularity due to their flexibility in designing the coil shape, potentially reliable and highly repeatable fabrication process, as well as their lightweight design [7], [8]. Moreover, PCB stators enable a modular design, leading to ease of maintenance, improved reliability, and cost efficiency. The modular design facilitates the creation of AFPM machines with a different number of phases by effortlessly stacking PCB stators without any major changes in the machine's geometry [4], [9]. The number of phases is typically determined by application requirements and the drive system [10].

A primary concern regarding PM machines, particularly in safety-critical applications such as electric aircraft propulsion systems, is their fault tolerance due to the inability to be de-excited, especially when connected to a prime mover. Extensive efforts have been undertaken to address this concern, focusing on both the machine itself and the power converter. This includes implementing corrective control strategies for power converters and control systems.

The combinations of slot and pole numbers that force the coupling between phases to be essentially zero have been previously investigated in [11]. This ensures that a fault in one phase does not adversely affect the remaining healthy phases, leading to improvements in fault tolerance. Practical combinations of slot and pole numbers for fault-tolerant permanent magnet brushless machines operating in multiplexed 2-phase and 3-phase configurations have been determined in [12]. A comprehensive literature review of proposed methods for improving fault tolerance in PM synchronous machines was presented in [13].

In this study, a two-phase coreless axial flux PM machine with modular PCB stators that are electrically insulated and magnetically decoupled is introduced. The magnetically decoupled phases prevent propagating faults from one phase to another, offering a high level of fault tolerance for the motor-drive system. Different inverter configurations for the introduced two-phase machine are also discussed to further improve the reliability of the system.

The performance of a prototyped two-phase and three-phase integral horsepower modular PCB stator coreless AFPM machine for high-speed applications was investigated and compared from various perspectives. The evaluation covers multiple facets, including the magnetic circuit, efficiency, power losses, torque and power density, torque ripple, design challenges, and control systems, providing a comprehensive understanding of the distinctions between these motors.

The performance of these motors was studied through 3D finite element analysis (FEA) developed in Ansys Electronics Desktop, utilizing the transient solution type [1], [14]. The accuracy of the models and FEA results was also experimentally verified with the available prototype machine in the laboratory. The introduced designs have great potential to be scaled to megawatt (MW) levels for electric aircraft applications, as presented in [15].

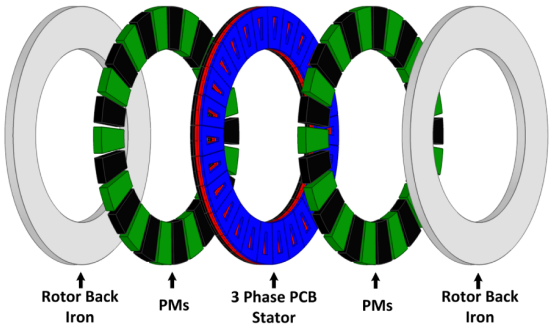

Fig. 1. The exploded view of the introduced double-rotor coreless AFPM machine with modular PCB stator, where each is dedicated to one phase. By stacking and mechanically shifting the PCB stators, multi-phase machines can be formed.

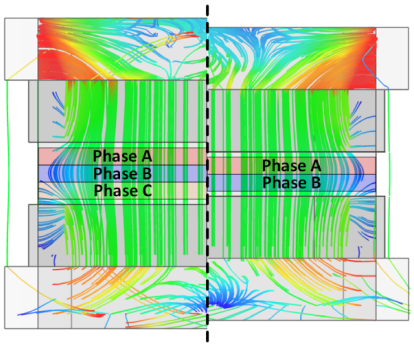

Fig. 2. Cross section view of the introduced three-phase and two-phase PCB stator machines. The mechanical airgap, i.e., the distance between magnet and PCB surfaces, is the same for both configurations.

II. Coreless AFPM Machines: Configurations and Modeling

Axial flux machines come in diverse configurations, with the dual rotor single-stator design being adopted for its robustness and superior torque density [3]. The exploded view of the under study double-rotor surface-mounted PM design with a three-phase PCB stator in the middle is illustrated in Fig. 1. Coreless stators can be designed with either conventional concentrated windings or distributed windings using Litz wires or PCB technologies.

Within conventional stator windings, distinct phase windings are placed on a common plane, with mechanical shifts equivalent of 72, 90, 120, and so forth, electrical degrees relative to each other, contingent upon the number of phases. Hence, to modify the number of phases, the stator needs to be redesigned, involving changes from the wiring to the alteration of the coil shape. Printed circuit board stators present an opportunity for implementing a modular design. In the realm of PCB stators, allocating one PCB to each phase winding not only ensures insulation between phases but also enhances simplicity in scaling.

In the aforementioned modular design, multi-phase machines can be created by stacking PCB stators and mechanically shifting them based on the number of phases and stator poles, as illustrated in Fig. 2, which depicts the two-phase and three-phase coreless AFPM machines under study. The fabricated PCB stators, exemplifying a two-phase and three-phase design, are depicted in Fig. 5b and Fig. 5c, respectively. The machine under study has 36 poles; hence, based on the basic equation $\theta_m = 2/p\ \theta_e$, the stacked PCBs need to be mechanically shifted by 5 and 6.66 degrees to form a two-phase and three-phase machine, respectively.

For a double rotor non-salient AFPM machine as shown in Fig. 1, the fundamental component of the airgap flux density in the axial direction can be represented as [16]:

$$B_{z,1}(\theta, z) = \hat{B} \cosh\left(\frac{\pi}{\tau_p} z\right) \cos(\theta)\,, \tag{1}$$

with the peak value:

$$\hat{B} = \frac{4B_r}{\pi} \frac{\sinh[\pi(k_\sigma k_b h_m/\tau_p)]}{\sinh[\pi(k_c g/2\tau_p)]} \sin\left(\frac{\pi}{2} k_m\right), \tag{2}$$

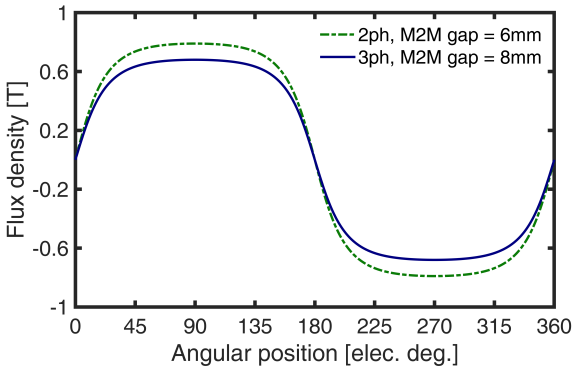

Fig. 3. The airgap flux density of the machines under study. The fundamental component of the airgap flux density is approximately 16% higher in the two phase machine due to the smaller magnet to magnet (M2M) gap.

where B_r is the remanence of the PMs, τ_p the pole pitch, h_m the magnet thickness, g the airgap length, and $k_m = \tau_m/\tau_p$ the pole-arc to pole-pitch ratio. The dimensions of the magnets, i.e., thickness, h_m, and arc length, τ_m, for a target airgap flux density and a specified magnet type can be decided [17].

Carter's and PM leakage coefficients are represented by k_σ and k_c, respectively. Both can be approximated with a unity value for surface PM (SPM) coreless machines. The coefficient k_b is equal to the number of PMs that provide the polar flux with a unity value for SPM.

For a given fundamental rated phase voltage, $\hat{V}_{ph,1}$, and considering the calculated magnetic flux density in the airgap, the number of turns per phase can be estimated as:

$$N_t = \frac{k_u\ \hat{V}_{ph,1}}{2\pi\ f_1\ \Psi_{PM}} = \frac{4p\ k_u\ \hat{V}_{ph,1}}{\pi^2 f_1\ k_{w1}\ k_{avg}\ k_m\ \hat{B}\ D_o^2\ (1-k_d^2)}, \tag{3}$$

where k_u is the ratio of back-EMF to induced voltage, usually near one for coreless machines, f_1 the rated fundamental frequency, p the number of pole-pairs, k_{w1} the fundamental winding factor, and k_{avg} the ratio of the fundamental to the average value of the airgap flux density; this can be approximated by $\pi/2$ or $1.1/k_m$ for SPM. In this equation, Ψ_{PM} denotes the open-circuit PM flux linkage.

The torque-producing component of the magnetic flux density (B_z) in the axial direction follows a hyperbolic sinusoidal

TABLE I

THE EXPERIMENTALLY MEASURED POWER LOSSES AND PERFORMANCE INDICES OF THE MACHINES UNDER STUDY WHILE DELIVERING THE SAME OUTPUT TORQUE OF 19 NM AT THE RATED SPEED OF 2100 RPM (4.18 KW).

Parameter	2ph	3ph	Unit
Torque constant	2.1	2.1	Nm/A
Current density	19.2	14.0	A/mm^2
Joule losses	143.4	129.5	W
Eddy current losses	26.2	22.6	W
Circ. current losses	≤ 1	≤ 1	W
Mechanical losses	30.4	30.4	W
Efficiency	95.4	95.8	%
Goodness	1.34	1.40	Nm/$\sqrt{W_{Loss}}$

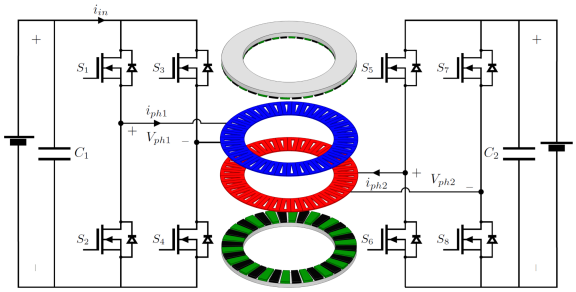

(a)

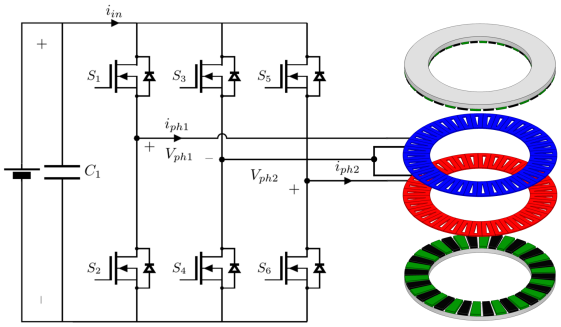

(b)

Fig. 4. Four-leg (a) and three-leg (b) two-phase inverters for the two-phase modular PCB stator coreless AFPM machine.

variation, exhibiting minima at the mid-airgap and increasing towards the permanent magnets on both sides (eq. 2). Due to a magnet-to-magnet gap difference of 2mm, the two-phase motor exemplified on the right side of Fig. 2 exhibits an approximately 16% higher fundamental component of the airgap flux density compared to the three-phase machine, as depicted in Fig. 3 based on FEA results.

The electromagnetic torque can be estimated by:

$$T_{em} = \frac{m}{2}\ p\ \Psi_{PM}\ J_{rms}\ SFF\ c_w\ \ell_c/N_t, \qquad (4)$$

where m is the number of phases, J_{rms} the current density in copper conductors, c_w the coil side width, ℓ_c the coil axial thickness, and SFF the slof-fill-factor.

Hence, according to (2) and (4), the two-phase machine delivers approximately 28% lower torque compared to the three-phase machine, within the same envelope (two-phase machine has a 2mm smaller axial length). In order to facilitate a fair comparison, the two-phase and three-phase machines need to be assessed while delivering the same torque and power. Consequently, the current density for the two-phase machine needs to be increased to compensate torque, leading to higher Joule losses within each PCB stator. It should be noted that Joule losses are not the only loss component within the stator windings. Coreless AFPM machines are subject to potentially high eddy and circulating current losses due to a lack of protection of stator teeth [5]. Therefore, efficiency and goodness (Nm/$\sqrt{W_{Loss}}$) are better performance indices to compare two-phase and three-phase configurations.

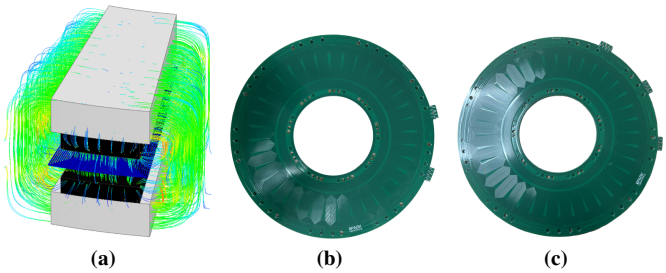

(a) (b) (c)

Fig. 5. The detailed 3D finite element model of 1/36 of the machine (a). The fabricated 36-pole PCB stators stacked up to form a two-phase (b) and a three-phase stator (c).

The total eddy current losses within PCB traces with rectangular cross sections can be calculated as:

$$P_{ed} = \frac{\pi^2\ N_{cs}\ N_t\ N_p\ f^2\ t_w\ t_h\ l_m}{6\rho}\left(t_w^2\ B_z^2 + t_h^2\ B_\phi^2\right), \qquad (5)$$

where N_{cs} represents the number of coil sides. The terms B_z and B_ϕ refer to the axial and tangential components of the flux density, respectively. Furthermore, t_w denotes the trace width, t_h represents the trace height in the z-direction, and f denotes the frequency of flux variations [5]. This equation implies that the eddy current losses are proportional to the square of the airgap flux density and the operating frequency.

III. FAULT-TOLERANT CAPABILITY, PERFORMANCE INVESTIGATION, AND RESULTS ANALYSIS

The loss components in the coreless axial flux permanent magnet (AFPM) machine prototype using two and three-phase stators were experimentally measured and separated at the rated current and speed of 2100rpm. This loss separation, as tabulated in Table I, enables a comprehensive comparison of the designs under study.

A smaller magnet-to-magnet gap in the two-phase configuration leads to a higher back-EMF. To maintain the back-EMF unchanged and avoid the need to change the drive system specifications, the number of turns per phase needs adjustment. To reduce Joule losses, the trace width can be increased within the same coil width when the number of turns is reduced.

The increase in eddy current losses due to wider traces can be mitigated by considering parallel conductors with added slits along the conductive tracks and/or using equivalent transposed conductors, as previously proposed in [18] and [8], respectively.

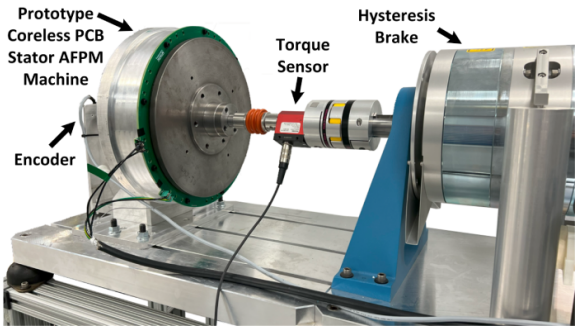

Fig. 6. The prototype 36-pole rotor with NdFeB permanent magnets mounted on the test bench. The machine was coupled to a hysteresis brake as a fully controllable mechanical load.

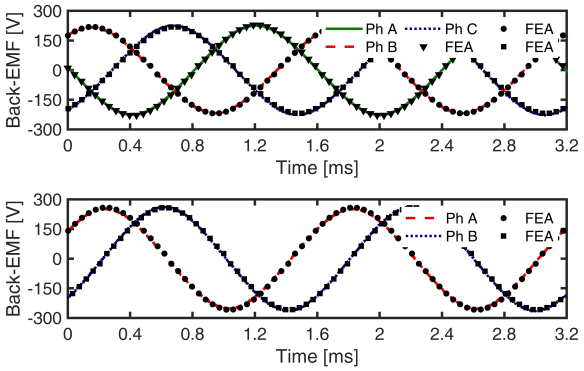

Fig. 7. The three-phase and two-phase machines back-EMFs derived form experimental tests and FEA.

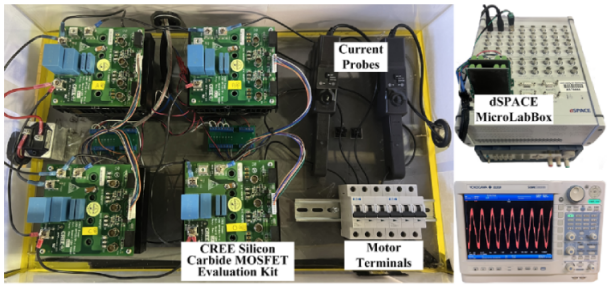

Fig. 8. The implemented four-leg two-phase drive system based on SiC MOSFETs for controlling the introduce two-phase machine.

The analysis of the results shows that the two-phase and three-phase configurations have comparable specific power and efficiency. In this case, assuming that eddy current losses are mitigated at the rated conditions when the machines are delivering 19Nm at 2100rpm, the three-phase machine has only a half-point higher efficiency.

There are no mutual inductances within the two-phase machine, as the flux generated by a current in one phase winding will not link to the other phase winding, which is displaced in space by 90 electrical degrees. The measured self and mutual inductances for both two-phase and three-phase machines are reported in Table II. Hence, potentially high current due to a fault in one phase does not propagate to another. Therefore, post-fault operation is ensured, provided that the very high torque ripple is acceptable within large inertia systems such as propellers and fans [19].

TABLE II
THE MEASURED SELF AND MUTUAL INDUCTANCES FOR BOTH THE TWO-PHASE AND THREE-PHASE MACHINES.

Configuration	L_{aa} $[\mu H]$	L_{ab} $[\mu H]$
Two Phase	33.4	0.0
Three Phase	32.3	11.6

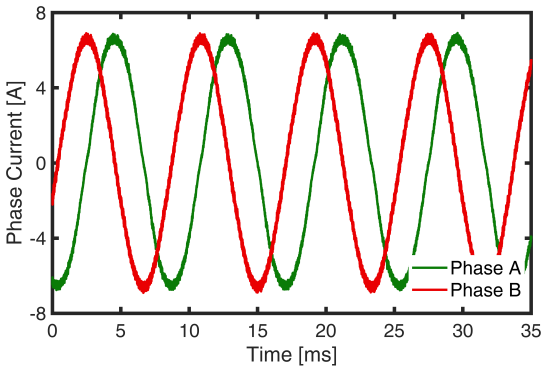

Fig. 9. The measured phase currents when the machine was controlled by the two-phase drive systems shown in Fig. 8.

To develop an effective cooling system, it is imperative to take into account the total power losses. Comparative analyses suggest that, from a cooling standpoint, there is negligible distinction between these two configurations. It is crucial to highlight that heat dissipation occurs on the surfaces of the PCBs. Consequently, despite the higher current density in one PCB stator within the two-phase machine resulting in a greater temperature rise, both machines' stators share the same surface area, and their cooling systems are identical.

Two common inverter configurations for two-phase machines are depicted in Fig. 4a and Fig. 4b [10]. The four-leg two-phase inverter, as illustrated in Fig. 4a, consists of two fully independent single-phase inverters, each connected to a distinct PCB stator (phase) and DC-link. In comparison to conventional three-leg two-phase inverters, as shown in Fig. 4b, which utilize six switches and are also employed in three-phase machines, the independent four-leg configuration exhibits a significantly elevated level of fault tolerance by decoupling each phase.

IV. Prototype Machine and Experimental Results

The performance of the two-phase machine was evaluated through experimental testing on the test bench depicted in Fig. 6. The prototype machine was coupled with a hysteresis brake as a mechanical load. The machine was powered by the two single-phase SiC-based 10 kW inverter shown in Fig. 8. The measured two-phase currents are nearly sinusoidal waveforms with negligible ripple, thanks to a high switching frequency of 65kHz as shown in Fig. 9. The two-phase and three-phase back-EMFs at the rated speed were measured and compared with the FEA results, showing very good agreement as illustrated in Fig. 7.

The output torque waveforms of the three-phase and two-phase machines when all phases are healthy and when one or two phases are lost due to a fault are shown in Fig 10. It needs to be highlighted that due to the high electrical and

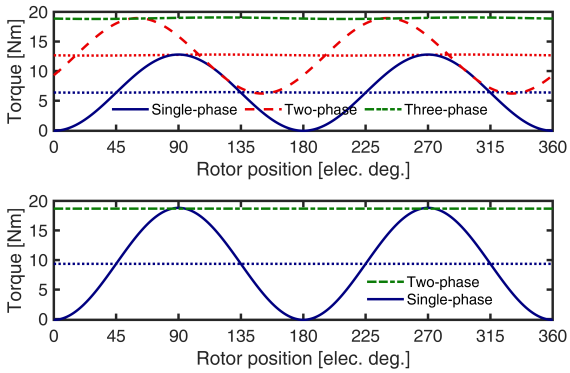

Fig. 10. The upper and lower figures show the FEA-based output torque waveforms of the three-phase and two-phase machines, respectively, under conditions where all phases are healthy, one phase is lost, and two phases are lost. The average values of the waveforms are plotted with dotted lines.

magnetic insulation between phases within the introduced two-phase machine, potential high currents due to a fault in one phase do not propagate to another, allowing the machine to continue its operation.

Within these two configurations, if a single-phase or two-phase stator fault occurs, the output torque undergoes pulsations with an always non-zero average and about 50% and 100% torque ripple, respectively. The substantial rotor inertia in axial flux machines, due to their very narrow axial direction compared to their large outer diameter, acts as a mechanical filter, effectively dampening the negative impacts on the machine performance.

V. Conclusion

In this paper, a fault-tolerant two-phase high-power coreless axial flux PM machine with a modular structure was proposed. The machine under study was a coreless AFPM machine with a PCB stator, providing a great opportunity for modular design where each phase was implemented on one single PCB stator. This modularity improves reliability, eases maintenance, and reduces downtime. Various converter configurations for controlling the introduced modular two-phase machine were also discussed.

The performance of the machine was compared to its three-phase counterpart through finite element analysis and experiments. The combined computational and experimental results indicate that the modular two-phase coreless machine has significantly better fault tolerance due to electrically and magnetically insulated phases, while maintaining comparable specific power and efficiency. In the case of phase loss the two-phase and three-phase machine produce pulsating torque with a non-zero average. High rotor inertia of axial flux machine is able to effectively filter out the negative impacts from this pulsating torque.

Acknowledgment

This paper is based upon work supported by the National Science Foundation (NSF) under Award No. #1809876. Any opinions, findings, conclusions, or recommendations expressed in this material are those of the authors and do not necessarily reflect the views of the NSF. The support of Ansys Inc., and of University of Kentucky, the L. Stanley Pigman Chair in Power Endowment is also gratefully acknowledged.

References

[1] M. Rosu, P. Zhou, D. Lin, D. Ionel, M. Popescu, F. Blaabjerg, V. Rallabandi, and D. Staton, *"Multiphysics Simulation by Design for Electrical Machines, Power Electronics and Drives"*, J. Wiley - IEEE Press, 2017.

[2] F. Nishanth, J. Van Verdeghem, and E. L. Severson, "A review of axial flux permanent magnet machine technology," *IEEE Transactions on Industry Applications*, vol. 59, no. 4, pp. 3920–3933, 2023.

[3] V. Rallabandi, N. Taran, D. M. Ionel, and J. F. Eastham, "Coreless multidisc axial flux pm machine with carbon nanotube windings," *IEEE Transactions on Magnetics*, vol. 53, no. 6, pp. 1–4, 2017.

[4] F. Marignetti, G. Volpe, S. M. Mirimani, and C. Cecati, "Electromagnetic design and modeling of a two-phase axial-flux printed circuit board motor," *IEEE Transactions on Industrial Electronics*, vol. 65, no. 1, pp. 67–76, 2018.

[5] Y. Chulaee, D. Lewis, A. Mohammadi, G. Heins, D. Patterson, and D. M. Ionel, "Circulating and eddy current losses in coreless axial flux PM machine stators with PCB windings," *IEEE Transactions on Industry Applications*, vol. 59, no. 4, pp. 4010–4020, 2023.

[6] D. Lawhorn, P. Han, D. Lewis, Y. Chulaee, and D. M. Ionel, "On the design of coreless permanent magnet machines for electric aircraft propulsion," in *2021 IEEE Transportation Electrification Conference Expo (ITEC)*, 2021, pp. 278–283.

[7] F. Marcolini, G. De Donato, F. G. Capponi, and F. Caricchi, "Design of a printed circuit board axial flux permanent magnet machine for high speed applications," *IEEE Transactions on Industry Applications*, pp. 1–11, 2024.

[8] Y. Chulaee, G. Heins, B. Robinson, M. Thiele, D. Patterson, and D. M. Ionel, "Design optimization considering a detailed pcb stator layout for coreless afpm machines with minimal eddy and circulating current losses," in *2023 IEEE Energy Conversion Congress and Exposition (ECCE)*, 2023, pp. 3753–3758.

[9] P. Han, D. Lawhorn, Y. Chulaee, D. Lewis, G. Heins, and D. M. Ionel, "Design optimization and experimental study of coreless axial-flux pm machines with wave winding pcb stators," in *2021 IEEE Energy Conversion Congress and Exposition (ECCE)*, 2021, pp. 4347–4352.

[10] D.-h. Jang, "PWM methods for two-phase inverters," *IEEE Industry Applications Magazine*, vol. 13, no. 2, pp. 50–61, 2007.

[11] A. Mitcham, "Favourable slot and pole number combinations for fault-tolerant pm machines," *IEE Proceedings - Electric Power Applications*, vol. 151, pp. 520–525(5), September 2004.

[12] J. Chai, J. Wang, K. Atallah, and D. Howe, "Performance comparison and winding fault detection of duplex 2-phase and 3-phase fault-tolerant permanent magnet brushless machines," in *2007 IEEE Industry Applications Annual Meeting*, 2007, pp. 566–572.

[13] A. M. EL-Refaie, "Fault-tolerant pm machines: A review," in *2009 IEEE International Electric Machines and Drives Conference*, 2009, pp. 1700–1709.

[14] *Ansys Electronics Desktop, Maxwell, version 23.1, 2023, ANSYS Inc.*

[15] D. D. Lewis, O. A. Badewa, A. Mohammadi, M. Vatani, and D. M. Ionel, "Fault tolerant electric machine concept for aircraft propulsion with pm rotor and dc current stator dual-stage excitation," in *2023 12th International Conference on Renewable Energy Research and Applications (ICRERA)*, 2023, pp. 607–611.

[16] Y. Chulaee, D. Lewis, M. Vatani, J. F. Eastham, and D. M. Ionel, "Torque and power capabilities of coreless axial flux machines with surface pms and halbach array rotors," in *2023 IEEE International Electric Machines Drives Conference (IEMDC)*, 2023, pp. 1–6.

[17] D. Ionel, J. Eastham, T. Miller, and E. Demeter, "Design considerations for permanent magnet synchronous motors for flux weakening applications," *IEE Proceedings-Electric Power Applications*, vol. 145, no. 5, pp. 435–440, 1998.

[18] G. François and B. Dehez, "Impact of slit configuration on eddy current and supply current losses in pcb winding of slotless pm machines," *IEEE Transactions on Industry Applications*, vol. 58, no. 5, pp. 6035–6044, 2022.

[19] M. Zafarani, E. Bostanci, Y. Qi, T. Goktas, and B. Akin, "Interturn short-circuit faults in permanent magnet synchronous machines: An extended review and comprehensive analysis," *IEEE Journal of Emerging and Selected Topics in Power Electronics*, vol. 6, no. 4, pp. 2173–2191, 2018.